

Study of the reduction and reoxidation of substoichiometric magnetite

M. Gotić*, G. Koščec, S. Musić

Division of Materials Chemistry, Ruđer Bošković Institute, P.O. Box 180, HR-10002 Zagreb, Croatia

ARTICLE INFO

Article history:

Received 7 October 2008
Received in revised form 24 October 2008
Accepted 27 October 2008
Available online 6 November 2008

Keywords:

Magnetite
Maghemite
Hematite
Stoichiometry
Mössbauer
FT-IR

ABSTRACT

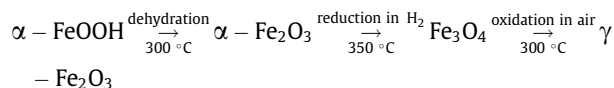
The commercial magnetite powder was characterised as substoichiometric magnetite ($\text{Fe}_{2.93}\text{O}_4$) with a small hematite fraction (~ 7 wt%). It consisted of micrometer-sized particles of regular (octahedral) and irregular morphologies. Reference sample was subjected to reduction by hydrogen gas and reoxidation at a temperature of up to 600 °C. The oxidation experiments were performed in an oxygen stream. Reference sample oxidised to a maghemite–hematite mixture, whereas the fraction of each phase was very sensitive to the oxidation temperature. XRD and FT-IR spectroscopy indicated the superstructure character of obtained maghemite samples with the ordering of cation vacancies in the maghemite crystal lattice. Mössbauer spectroscopy was very sensitive to magnetite stoichiometry, however, it could not detect less than 10 wt% of hematite in the maghemite–hematite mixture. In reduction experiments, conditions for the reduction of reference sample to stoichiometric magnetite ($\text{Fe}_{3.00}\text{O}_4$) were found. The reduction was performed by hydrogen gas under static conditions (375 °C, 150 min). Under this static condition the relatively high amount of water condensed inside the evacuated quartz tube. The formation of water is due to the chemisorption of hydrogen molecules on the iron oxide, which then dissociate from iron oxide generating an intermediate hydroxyl group according to the general equations: $2\text{O}^{2-}(\text{s}) + \text{H}_2(\text{g}) \rightarrow 2\text{OH}^-(\text{s}) + 2\text{e}^-$ and $2\text{OH}^-(\text{s}) \rightarrow \text{O}^{2-}(\text{s}) + \square_{\text{a}} + \text{H}_2\text{O}(\text{g})$, where (s) signifies a solid (hematite or substoichiometric magnetite), (g) a gas phase and \square_{a} an anionic vacancy formed in hematite or substoichiometric magnetite. Thus, in order to ensure a good reduction condition, water vapour was removed from the quartz tube and the tube was refilled with hydrogen gas every 30 min.

© 2008 Elsevier B.V. All rights reserved.

1. Introduction

Synthetic iron oxides [1–5] (a group name for iron oxyhydroxides and oxides) are important materials with numerous applications. Amongst them, magnetite (Fe_3O_4) and maghemite ($\gamma\text{-Fe}_2\text{O}_3$) are ferrimagnetic at room temperature and they possess unique electric and magnetic properties. They are widely used as material in catalysis, magnetic separation, ceramics processing, energy and magnetic data storage, and as protection against microwave radiation. Moreover, both magnetite and maghemite have been extensively investigated for application in biomedicine [6,7]. For example, they have been recognised as suitable magnetic materials for MR imaging, drug delivery, drug targeting, cell labelling and magnetic separation, as well as a hyperthermia agent. Magnetite has better magnetic properties than maghemite, however, magnetite tends to oxidise easily due to the presence of Fe^{2+} , whereas maghemite is chemically and physically very stable. The oxidation of magnetite deteriorates its magnetic properties. The common process for the preparation of maghemite starts from acicular precursor crystals of either non-magnetic $\alpha\text{-FeOOH}$ (goe-

thite) or non-magnetic $\gamma\text{-FeOOH}$ (lepidocrocite) [8]; these are dehydrated directly to $\alpha\text{-Fe}_2\text{O}_3$ (hematite) and further reduced to Fe_3O_4 (magnetite). Magnetite is then carefully oxidised to yield ferrimagnetic acicular $\gamma\text{-Fe}_2\text{O}_3$ (maghemite) particles. Schematically the process can be shown as follows:

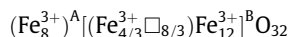


Generally, the maghemite particles thus obtained showed high saturation magnetization and high coercivity due to their shape anisotropy. However, each of the above steps is important, since the magnetic properties of the final product depend on particle size, morphology, crystallinity and present impurities. Hematite is the most frequent impurity accompanying maghemite. The presence of hematite may significantly disturb the magnetic properties of maghemite.

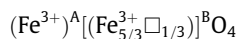
Magnetite (Fe_3O_4) has an inverse spinel structure in which cations occupy tetrahedral and octahedral sites in the face-centred cubic close-packed oxygen lattice [9,10]. Stoichiometric magnetite contains eight Fe^{3+} at tetrahedral (8a) or A-sites and 16 cations ($8\text{Fe}^{3+} + 8\text{Fe}^{2+}$) at octahedral (16d) or B-sites. Fe^{2+} ions in stoichiometric magnetite easily oxidise to form the structure deficient

* Corresponding author. Tel.: +385 1 4561 123.
E-mail address: gotic@irb.hr (M. Gotić).

in Fe^{2+} , i.e., the nonstoichiometric magnetite ($\text{Fe}_{3-x}\text{O}_4$). When all Fe^{2+} cations in the nonstoichiometric magnetite are oxidised the $\text{Fe}_{2.67}\text{O}_4$ compound known as maghemite ($\gamma\text{-Fe}_2\text{O}_3$) is obtained. The stoichiometric formula of maghemite [11,12] can be written as



Or equivalently as



(where $()$ stands for the tetrahedral or A-sites, $[]$ stands for the octahedral or B-sites and \square denotes the cation vacancies. The vacancies in maghemite are located on the octahedral B-sites exclusively, or on the both tetrahedral A-sites and octahedral B-sites [13,14], which establish a neutral charge of the whole structure. It has been suggested that the vacancies can be distributed [15–21] (i) at random (space group $Fd\bar{3}m$); (ii) ordered as the lithium cation in LiFe_5O_8 (space group $P4_132$); and (iii) with an ordered distribution with tetragonal symmetry (space group $P4_32_12$). It has also been shown that infrared spectroscopy is very sensitive to the order–disorder distribution of the cationic vacancies in the maghemite structure [16,20].

In this work, micrometer-size magnetite particles as a model system were subjected to reduction and reoxidation at a temperature of up to 600 °C. The reduction of magnetite by hydrogen was performed under static conditions, whereas the oxidation experiments were performed in an oxygen stream. Samples were characterised using field emission scanning electron microscopy (FE SEM), X-ray diffraction (XRD), Fourier transform infrared spectroscopy (FT-IR) and Mössbauer spectroscopy. The sensitivity of each technique in the structural characterisation of maghemite and stoichiometric magnetite as well as in the detection of hematite impurity is discussed.

2. Experimental

Iron (II, III) oxide, supplied by Ventron, 99.5%, spectroscopically pure KBr supplied by Merck and commercial gases H_2 and O_2 of analytical purity supplied by Messer Croatia Plin were used.

The starting chemical supplied by Ventron was used in the reduction and reoxidation experiments. Experimental conditions for the preparation of reduced and reoxidised samples are given in Table 1.

In order to obtain stoichiometric magnetite the starting chemical (sample M-0) was dried under vacuum at room temperature, then put into a quartz tube. The quartz tube was properly evacuated and then overfilled with H_2 . Thus prepared the quartz tube was put into a tubular furnace and heated to the predetermined temperature (static-hydrogen condition, heating up to 375 °C). In

order to remove water vapour released during the sample heating under static-hydrogen conditions, the quartz tube was evacuated

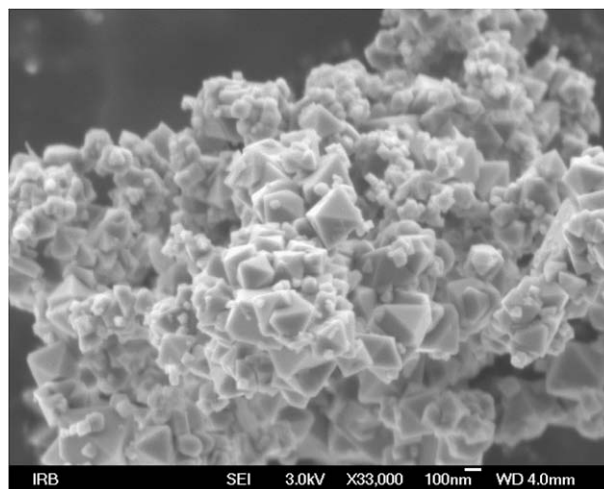


Fig. 1. Field emission scanning electron microscopy (FE SEM) images of reference sample M-0. Micrometer-sized particles of regular (octahedral) and irregular morphologies are visible.

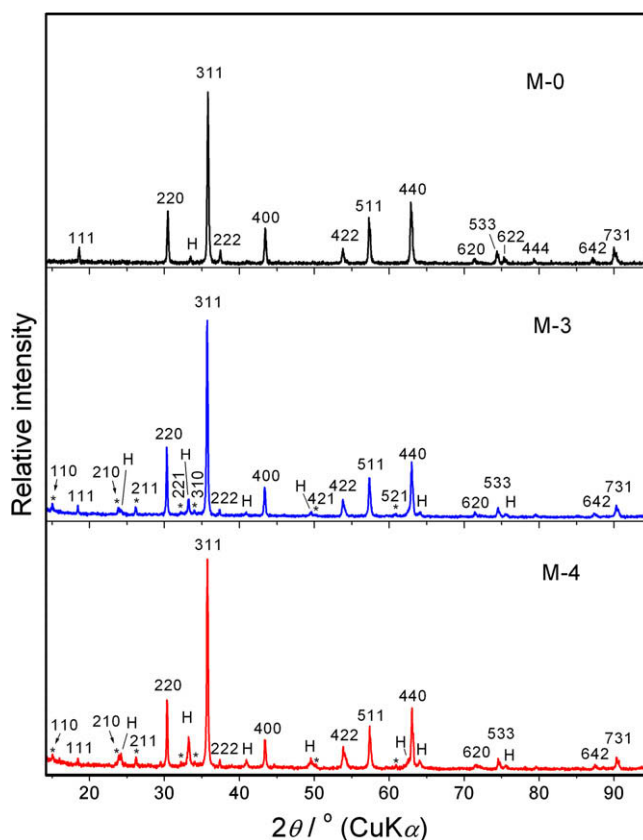


Fig. 2. XRD patterns of reference sample M-0 and oxidised samples M-3 and M-4. Reference sample M-0 is assigned in accordance with the JCPDS card 19-0629 (magnetite). The hkl indices of magnetite (space group $Fd\bar{3}m$) are given. The presence of a small quantity of hematite (JCPDS card 33-0664) as impurity is also detected in reference sample M-0. The XRD patterns of samples M-3 and M-4 are assigned in accordance with the JCPDS card 39-1346 (maghemite). The hkl indices of maghemite, space group $P4_132$ are given. The peaks not present in XRD patterns of magnetite are marked with asterisks. Hematite peaks are marked with H.

Table 1
Experimental conditions for the preparation of samples M-1 to M-12.

Sample	Time of heating (min)	Temperature of heating (°C)	Bubbling with O_2	H_2 atmosphere
M-0	–	–	–	–
M-1	10	250	Yes	–
M-2	30	250	Yes	–
M-3	120	250	Yes	–
M-4	1440	250	Yes	–
M-5	2880	250	Yes	–
M-6	30	200	Yes	–
M-7	30	300	Yes	–
M-8	30	400	Yes	–
M-9	30	600	Yes	–
M-10	30	250	–	Yes
M-11	150	300	–	Yes
M-12	150	375	–	Yes

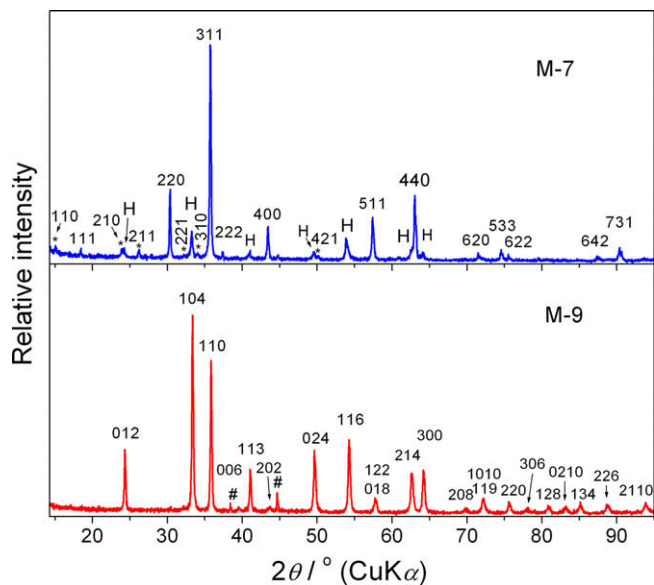


Fig. 3. XRD patterns of samples M-7 and M-9. Sample M-7 is assigned in accordance with the JCPDS card 39-1346 (maghemite) and the JCPDS card 33-0664 (hematite). The *hkl* indices of maghemite are indicated. The peaks not present in XRD patterns of magnetite are marked with asterisks. Sample M-9 is assigned as pure hematite. The *hkl* indices of hematite are indicated. The two lines marked # are due to the sample holder.

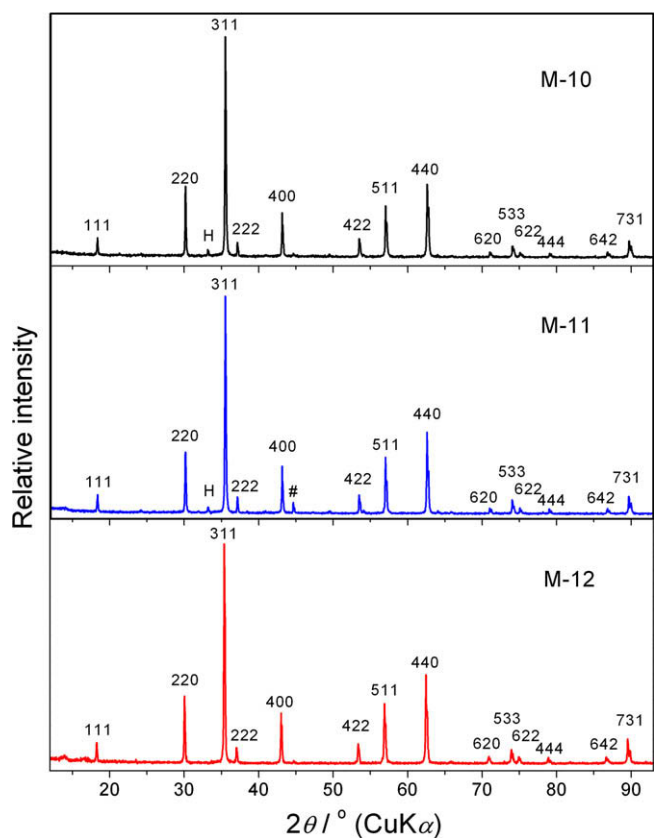


Fig. 4. XRD patterns of samples M-10, M-11 and M-12, prepared under the reduction of reference sample M-0 in hydrogen atmosphere. Samples M-10 and M-11 correspond to substoichiometric magnetite with a small hematite fraction, whereas sample M-12 is characterised as stoichiometric magnetite. The *hkl* indices of magnetite are indicated. Hematite peaks are marked with H. The line marked # is due to the sample holder.

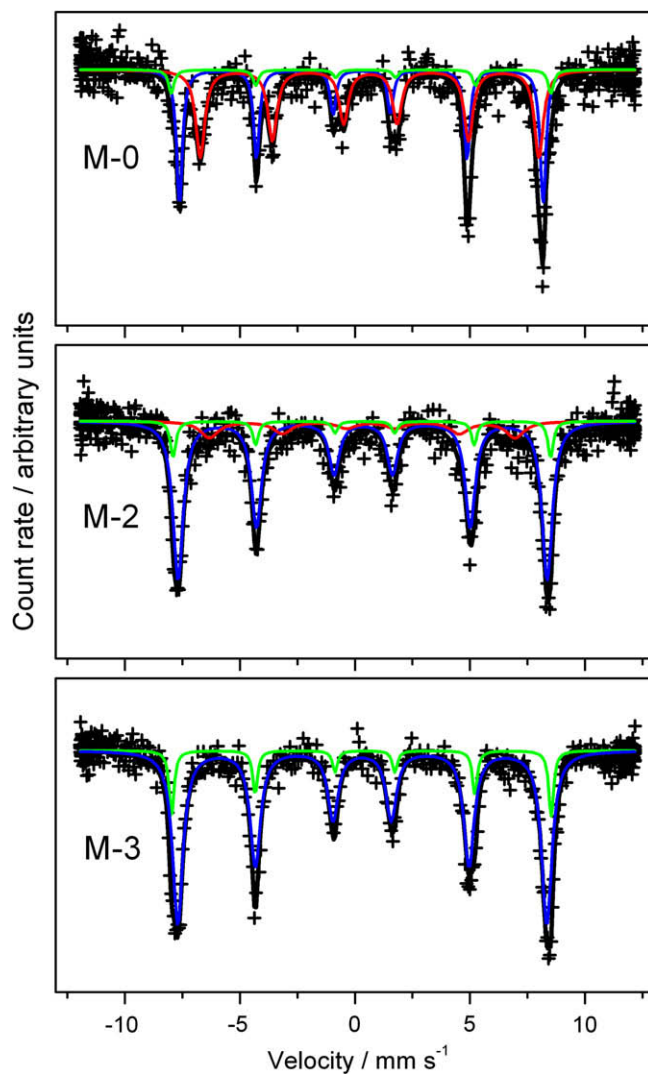


Fig. 5. Mössbauer spectra of samples M-0, M-2 and M-3 recorded at 20 °C. The Mössbauer spectrum of sample M-0 is fitted for three sextets. The outermost small sextet belongs to hematite and the other two sextets correspond to magnetite. The inner sextet of magnetite is due to Fe²⁺ and Fe³⁺ ions at the octahedral B-site. With the oxidation the inner sextet of magnetite decreases (sample M-2) and then completely disappears (sample M-3). Mössbauer parameters are given in Table 2.

every 30 min and refilled with hydrogen. Temperature in the tubular furnace was controlled by a digital thermocouple thermometer.

The reoxidation of sample M-0 was performed in the tubular furnace under the flow of pure O₂. Temperature in the tubular furnace was measured directly by the thermometer (up to 500 °C).

The ⁵⁷Fe Mössbauer spectra were recorded in the transmission mode using a standard instrumental configuration by *WissEl GmbH* (Starnberg, Germany). The ⁵⁷Co in the rhodium matrix was used as a Mössbauer source. The spectrometer was calibrated at 20 °C using the standard α -Fe foil spectrum. The velocity scale and all the data refer to the metallic α -Fe absorber at 20 °C. The experimentally observed Mössbauer spectra were fitted using the *MossWinn* program.

The FT-IR spectra were recorded at 20 °C using a *Perkin-Elmer* spectrometer model 2000. The FT-IR spectrometer was coupled with a personal computer loaded with the IRDM (IR data manager) program to process the recorded spectra. The specimens were pressed into small discs using a spectroscopically pure KBr matrix. The spectra were recorded using a KBr beam splitter in the mid IR region (4000–400 cm⁻¹) and a Mylar beam splitter in the far IR region (700–200 cm⁻¹).

Table 2
⁵⁷Fe Mössbauer parameters at 20 °C calculated for selected samples using the MossWinn program.

Sample	Assignment	IS (mm s ⁻¹)	QS (mm s ⁻¹)	B _{hf} (T)	LW (mm s ⁻¹)	Relative area A/%	Stoichiometry	Chi
M-0	M1	0.29	-0.02	49.0	0.31	42.0	Fe _{2.93} O ₄	1.31
	M2	0.66	-0.04	45.7	0.47	51.0		
	H	0.37	-0.2	51.2	0.29	7.0	α-Fe ₂ O ₃	
M-1	M1	0.31	-0.01	49.6	0.51	67.3	Fe _{2.79} O ₄	1.82
	M2	0.51	-0.19	42.5	1.50	23.9		
	H	0.37	-0.13	51.0	0.29	8.8	α-Fe ₂ O ₃	
M-2	M1	0.35	-0.03	49.8	0.54	76.1	Fe _{2.74} O ₄	1.25
	M2	0.51	-0.37	41.2	0.94	14.6		
	H	0.37	-0.13	50.9	0.29	9.3	α-Fe ₂ O ₃	
M-3	MH1	0.32	-0.01	49.7	0.54	85.3	γ-Fe ₂ O ₃	1.41
	H	0.36	-0.15	51.1	0.26	14.7	α-Fe ₂ O ₃	
M-6	M1	0.32	0.01	49.5	0.48	64.1	Fe _{2.80} O ₄	1.30
	M2	0.65	-0.02	45.4	0.65	26.6		
	H	0.37	-0.13	51.0	0.28	9.3	α-Fe ₂ O ₃	
M-7	MH1	0.32	-0.01	49.7	0.54	81.8	γ-Fe ₂ O ₃	1.31
	H1	0.36	-0.15	51.4	0.24	18.2	α-Fe ₂ O ₃	
M-8	H1	0.37	-0.17	51.4	0.29	54.0	α-Fe ₂ O ₃	1.11
	MH1	0.34	-0.05	49.5	0.60	46.0	γ-Fe ₂ O ₃	
M-10	M1	0.33	-0.04	49.1	0.35	43.2	Fe _{2.93} O ₄	1.12
	M2	0.69	0.00	45.6	0.51	50.7		
	H	0.37	-0.13	51.1	0.29	6.1	α-Fe ₂ O ₃	
M-11	M1	0.27	-0.02	48.9	0.29	35.2	Fe _{2.98} O ₄	1.30
	M2	0.66	0.01	45.9	0.41	60.3		
	H	0.36	-0.13	51.4	0.29	4.4	α-Fe ₂ O ₃	
M-12	M1	0.27	-0.02	48.8	0.27	33.6	Fe _{3.00} O ₄	1.32
	M2	0.66	0.02	45.8	0.38	66.4		

Key: IS = isomer shift given relative to α-Fe at 20 °C; QS = quadrupole shift; B_{hf} = hyperfine magnetic field; LW = line width; Chi = goodness of fitting (1.00 = relatively very good fitting; 2.00 = relatively weak fitting).

Error: IS = ±0.01 mm s⁻¹; QS = ±0.01 mm s⁻¹; B_{hf} = ±0.2 T.

Remarks: M1 = outer sextet of magnetite; M2 = inner sextet of magnetite; MH1 = sextet of maghemite; H = sextet of hematite.

The XRD patterns were recorded at RT using APD 2000 X-ray powder diffractometer (CuKα radiation, graphite monochromator, NaI-Tl detector) manufactured by *ItalStructures*, Riva Del Garda, Italy.

The thermal field emission scanning electron microscope (FE SEM, model JSM-7000F), manufactured by *Jeol Ltd.*, was linked to the EDS/INCA 350 (energy dispersive X-ray analyzer) manufactured by *Oxford Instruments Ltd.*

3. Results and discussion

In the present work, the commercial magnetite powder (sample M-0) was subjected to reduction and reoxidation at a temperature of up to 600 °C. Fig. 1 shows the FE SEM micrographs of reference sample M-0. It consists of micrometer-size particles of regular (octahedral) and irregular morphologies. The morphology of the particles did not change significantly while heated up to 400 °C.

Fig. 2 shows XRD patterns of reference sample M-0 and oxidised samples M-3 and M-4. Reference sample M-0 is assigned in accordance with the JCPDS card 19-0629 (magnetite). The declared magnetite cell constant is $a = 8.396 \text{ \AA}$. The calculated cell constant of reference sample M-0 is $a = 8.373 \text{ \AA}$ and can be characterised as substoichiometric magnetite.

The hkl indices of magnetite (space group $Fd\bar{3}m$) are given. The of a small quantity (~7 wt%) of hematite (JCPDS card 33-0664) as impurity is also detected in reference sample M-0. The XRD patterns of samples M-3 and M-4 are assigned in accordance with the JCPDS card 39-1346 (maghemite). The hkl indices of maghemite, space group $P4_132$ are given. The peaks not present in the XRD patterns of magnetite are marked with asterisks. These extra peaks indicate the ordering of cation vacancies in the maghemite

crystal lattice. The XRD patterns of maghemite and magnetite are very much alike, so very often these two phases cannot be distinguished by XRD. This is because the structural properties of maghemite depend on the preparation conditions. If maghemite crystallises in cubic space group $Fd\bar{3}m$ (the vacancies are distributed at random), the XRD patterns of maghemite and magnetite will be virtually the same, the only difference being in their lattice constant which is smaller for maghemite than for magnetite. If maghemite crystallises in cubic symmetry, space group $P4_132$ or tetragonal symmetry, space group $P4_32_12$ (cation vacancy ordering), its XRD patterns should differ from the XRD patterns of magnetite due to the presence of extra superstructure peaks. Likewise, the superstructure peaks were observed in the nanocrystalline maghemite. Nevertheless, the good model system chosen in this work (micrometer-size particles of good crystallinity) and the good statistics of collected XRD patterns easily demonstrated the extra XRD lines of maghemite in comparison with magnetite. The amount of hematite in samples M-3 and M-4 increased with the heating temperature, but not in excess of about 28% upon 24 h of heating at 250 °C. Thus, the time of heating is not a determining factor for the maghemite-to-hematite transition.

Fig. 3 shows the XRD patterns of samples M-7 and M-9 oxidised at 300 and 600 °C for 30 min, respectively. Sample M-7 is a mixture of maghemite and hematite, whereas sample M-9 is a pure hematite. The conversion of magnetite/maghemite to hematite is highly sensitive to temperature increase.

Fig. 4 shows the XRD patterns of samples M-10, M-11 and M-12 obtained under the reduction of reference sample M-0 in hydrogen atmosphere. Samples M-10 and M-11 correspond to substoichiometric magnetite with a small hematite fraction, whereas sample M-12 is characterised as stoichiometric magnetite. The lattice constants are $a = 8.373 \text{ \AA}$, $a = 8.376 \text{ \AA}$ and $a = 8.400 \text{ \AA}$ for samples

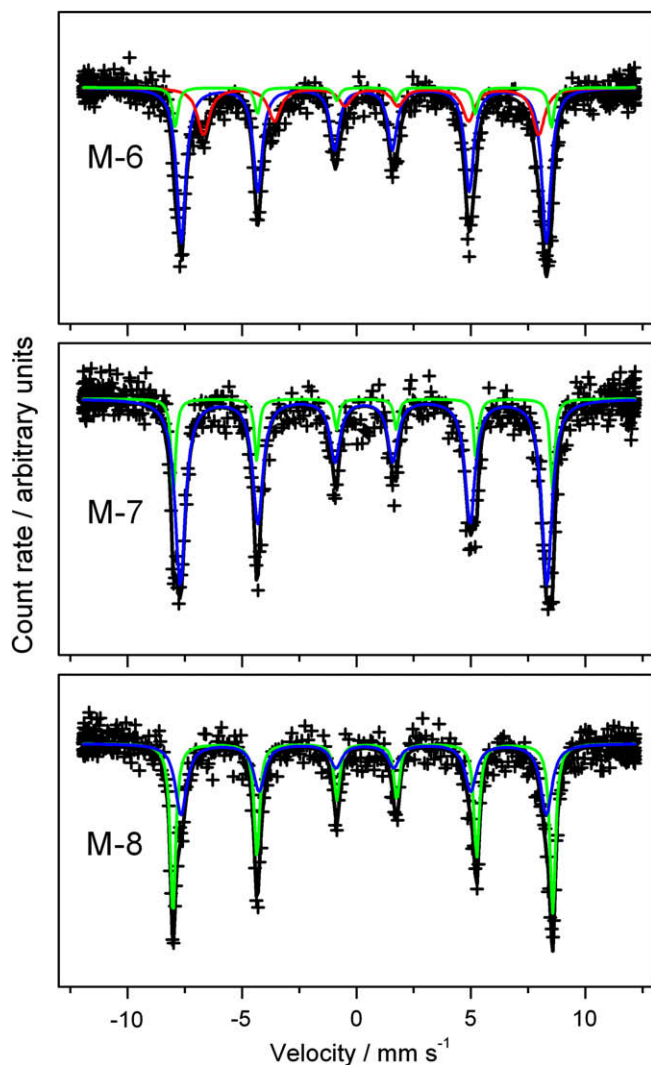


Fig. 6. Mössbauer spectra of oxidised samples M-6, M-7 and M-8 recorded at 20 °C. With the increase in oxidation temperature substoichiometric magnetite with a small hematite fraction (sample M-6) rapidly oxidised to a maghemite–hematite mixture (sample M-7). Hematite is a dominant phase in sample M-8. Mössbauer parameters are given in Table 2.

M-10, M-11 and M-12, respectively. On the basis of lattice constants, the approximate stoichiometries for samples M-10, M-11 and M-12 are $\text{Fe}_{2.86}\text{O}_4$, $\text{Fe}_{2.87}\text{O}_4$ and $\text{Fe}_{3.00}\text{O}_4$, respectively.

Fig. 5 shows the Mössbauer spectra of samples M-0, M-2 and M-3 recorded at 20 °C. The Mössbauer spectrum of sample M-0 is fitted with three sextets. The outermost small sextet belongs to hematite [10,22] and the other two sextets correspond to magnetite. The outer magnetite sextet belongs to Fe^{3+} ions at the tetrahedral sites, whereas the inner magnetite sextet is due to Fe^{2+} and Fe^{3+} ions at the octahedral B-site. At room temperature the electron exchange between these two oxidation states occurs faster ($\tau \sim 1$ ns) than the decay of the excited state of ^{57}Fe ($\tau \sim 98$ ns) and for that reason the inner magnetite sextet is fitted to the average charged $\text{Fe}_B^{2.5+}$. The ratio of relative surface areas of the inner and outer sextets is a good measure of the magnetite (non)stoichiometry. The calculated stoichiometry and other Mössbauer parameters for all samples investigated in this work are given in Table 2. The stoichiometry of reference sample M-0 is $\text{Fe}_{2.93}\text{O}_4$ and with oxidation it drops to $\text{Fe}_{2.74}\text{O}_4$ in sample M-2. With further oxidation the inner magnetite sextet disappeared, which proved a complete conversion of substoichiometric magnetite to maghemite. In

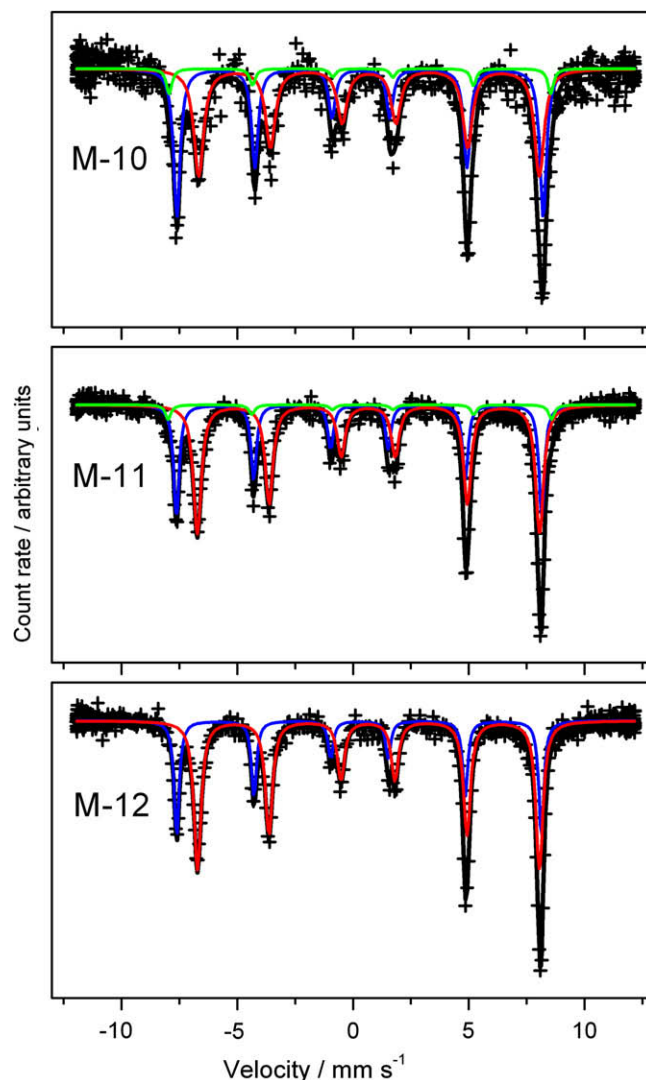


Fig. 7. Mössbauer spectra of samples M-10, M-11 and M-12 obtained upon reduction of reference sample M-0 in hydrogen atmosphere. The spectra were recorded at 20 °C. The sextet corresponding to hematite was introduced on the basis of XRD results. The magnetite stoichiometry changed from substoichiometric $\text{Fe}_{2.93}\text{O}_4$ in sample M-10 to stoichiometric $\text{Fe}_{3.00}\text{O}_4$ in sample M-12. Mössbauer parameters are given in Table 2.

this work the Mössbauer spectrum of maghemite is fitted to one sextet. The hematite sextet in samples M-0 and M-2 is introduced on the basis of XRD results. In other words, because of the similar parameters for outer sextet of magnetite and sextet of hematite, the presence of less than 10 wt% of hematite in the mixture of substoichiometric magnetite/hematite or powder mixtures of maghemite/hematite was not detectable with Mössbauer spectroscopy.

Fig. 6 shows the Mössbauer spectra of oxidised samples heated in an oxygen stream at 200, 300 and 400 °C for 30 min (samples M-6, M-7 and M-8, respectively). With the increase in temperature the substoichiometric magnetite rapidly oxidised and the hematite fraction increased, which is in accordance with XRD results.

Fig. 7 shows the Mössbauer spectra of samples M-10, M-11 and M-12 prepared upon reduction of reference sample M-0 in hydrogen atmosphere. The sextet corresponding to hematite was introduced on the basis of XRD results. The magnetite stoichiometry changed from substoichiometric $\text{Fe}_{2.93}\text{O}_4$ in sample M-10 to stoichiometric $\text{Fe}_{3.00}\text{O}_4$ in sample M-12. These results are in accordance with XRD results; however, the magnetite stoichiometry obtained by Mössbauer spectroscopy is more stoichiometric than

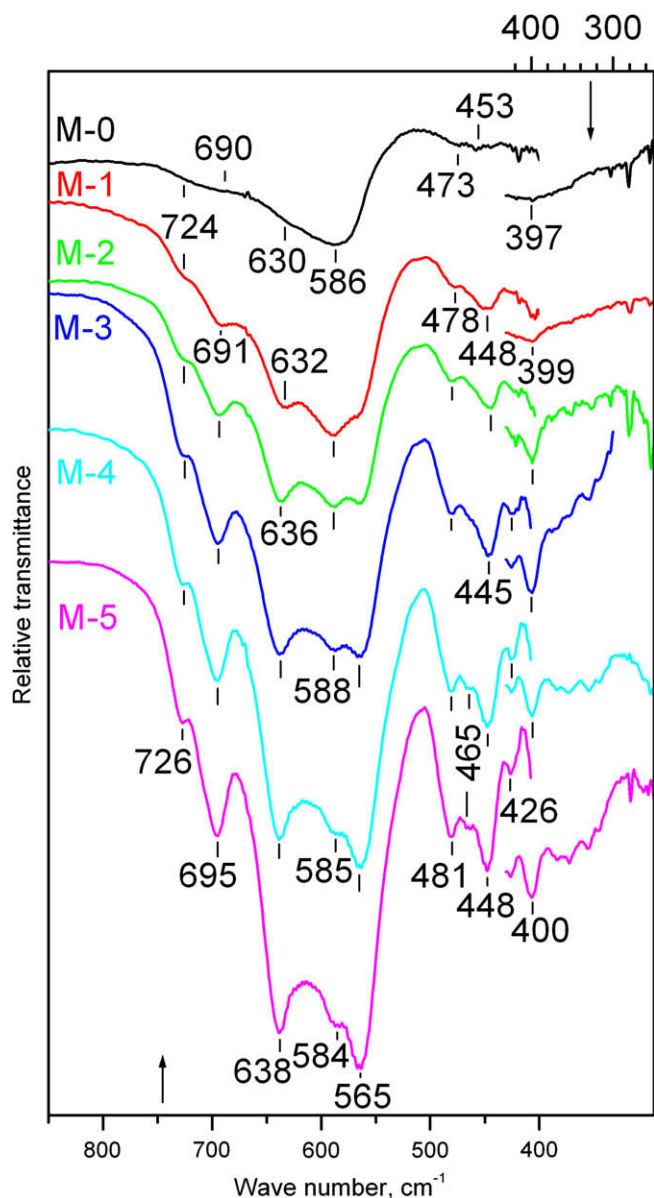


Fig. 8. FT-IR spectra of reference sample M-0 and oxidised samples M-1, M-2, M-3, M-4 and M-5. The spectra were recorded using a KBr beam splitter in the mid IR region (lower scale) and a Mylar beam splitter in the far IR region (upper scale).

that obtained by XRD. By contrast, the calculated stoichiometry for sample M-12 using Mössbauer spectroscopy and XRD matched perfectly, and strictly speaking corresponded to a little over-stoichiometric magnetite in both cases.

Fig. 8 shows the FT-IR spectra of reference sample M-0 and oxidised samples M-1, M-2, M-3, M-4 and M-5. The spectra were recorded using a KBr beam splitter in the mid IR region (lower scale) and a Mylar beam splitter in the far IR region (upper scale). Reference sample M-0 is characterised by a strong band at 586 cm^{-1} , not well-resolved bands at 473 and 453 cm^{-1} and shoulders at 724 , 690 and 630 cm^{-1} . In the far infrared region a band at 397 cm^{-1} is present. Group theoretical calculations predicted four IR active modes in the vibrational spectra of the inverse cubic spinels (magnetite) with two main bands at 570 and 360 cm^{-1} and another two at lower wave numbers, which were difficult to observe due to low intensity. Thus the band at 586 cm^{-1} is assigned to the ν_1 Fe–O stretching mode of the tetrahedral and octahedral sites and the

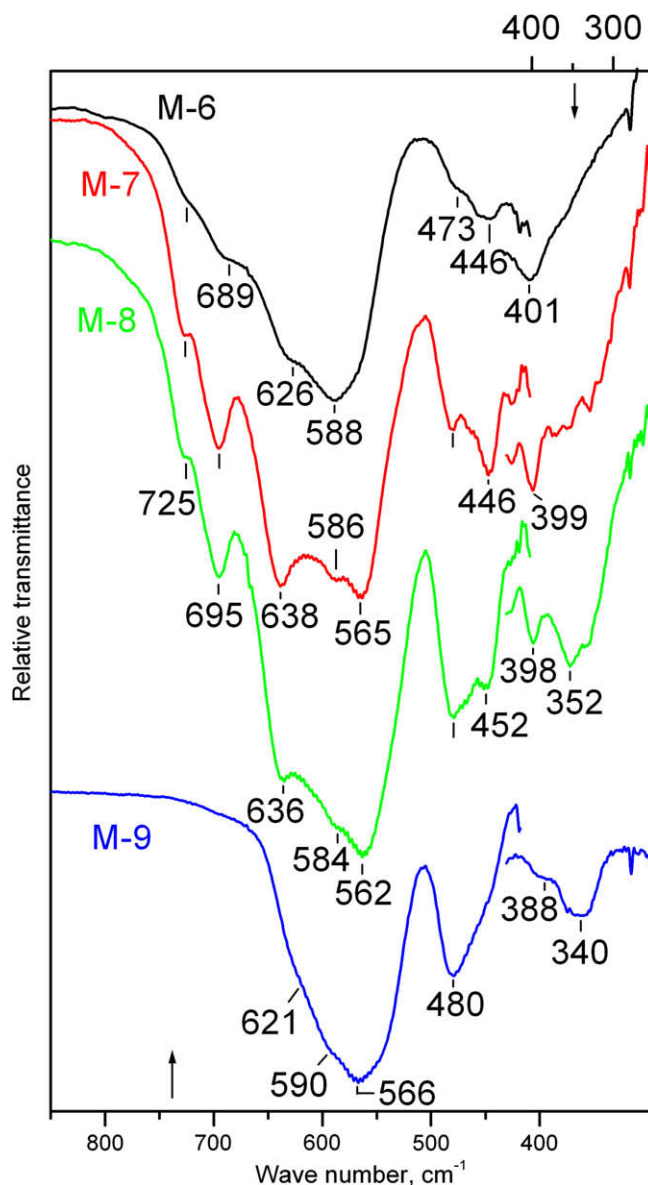


Fig. 9. FT-IR spectra for samples M-6 to M-9 prepared by the oxidation of reference sample M-0 at different temperatures (200 – $600\text{ }^\circ\text{C}$) for the same period of time (30 min).

band at 397 cm^{-1} is assigned to the ν_2 Fe–O stretching mode of the octahedral sites of the magnetite crystal lattice [23,24]. The additional bands in the FT-IR spectrum of reference sample M-0 are due to magnetite nonstoichiometry. The confirmation for this is the fact that the IR bands of maghemite in sample M-1 fit in very well with the shoulders in reference sample M-0. The FT-IR spectroscopy is highly sensitive to the short range order and thus can detect an early change in the local symmetry of magnetite. In the present case, with the oxidation of substoichiometric magnetite (sample M-0) to maghemite (samples M-1 to M-5) the crystal lattice symmetry changed from cubic symmetry, space group $Fd\bar{3}m$ to cubic symmetry, space group $P4_132$. This decrease in symmetry is induced by the ordering of cation vacancies and as a result a new set of bands forbidden in the inverse spinel cubic group $Fd\bar{3}m$ appeared in FT-IR spectrum at 726 , 695 , 638 , 584 , 565 , 481 , 465 , 448 , 426 and 400 cm^{-1} . In our earlier work we managed to synthesise pure $\gamma\text{-Fe}_2\text{O}_3$ by thermal decomposition of a mixture of Fe(II)-

and Fe(III)-oxalate salts and the FT-IR spectrum of that sample was virtually identical to the FT-IR spectra of samples M-3 to M-5. Moreover, in the FT-IR spectrum of pure γ -Fe₂O₃ a band at 609 cm⁻¹ was also present (sample S₁₅ in Ref. [1]). This band at 609 cm⁻¹ is not observed in the FT-IR spectra of samples M-1 to M-5 due to the presence of hematite impurity. The assignments of FT-IR bands for samples M-1 to M-5 are in accordance with XRD results and the cation vacancy ordering found in other studies. Also, the FT-IR spectrum of nanocrystalline maghemite showed the same characteristic.

Fig. 9 shows the evolution of FT-IR spectra for samples M-6 to M-9 that were oxidised at different temperatures (200–600 °C). The FT-IR spectrum of sample M-6 contains the maghemite bands (725, 689, 626, 473 and 446 cm⁻¹), but basically resembles that of nonstoichiometric magnetite with intensive and broad bands at 588 and 401 cm⁻¹. With an increase in oxidised temperature the FT-IR band of maghemite fully developed, however, the absence of a band at about 609 cm⁻¹ indicated a hematite impurity in sample M-7. With further increase in oxidised temperature the band of maghemite at 638 cm⁻¹ slightly shifted to the lower wave numbers and its relative intensity decrease thus indicated a higher hematite impurity fraction in sample M-8. At 600 °C the pure hematite formed (sample M-9) and its FT-IR spectrum is characterised by shoulders at 621, 590 and 388 cm⁻¹ and broad bands at 566, 480 and 340 cm⁻¹.

Fig. 10 shows the FT-IR spectra of samples M-10, M-11 and M-12 that were prepared upon reduction of reference sample M-0 in hydrogen atmosphere under static conditions. The FT-IR spectrum of sample M-10 is similar to reference sample M-0 due to the substoichiometric nature of this sample obtained in a weak reductive condition. Sample M-11 was prepared under a better reductive condition and its FT-IR spectrum does not contain a shoulder at 688 cm⁻¹. Both samples, M-10 and M-11, contained small quantities of hematite impurity as determined by XRD. Sample M-12 corresponds to stoichiometric magnetite (XRD and Mössbauer analyses) and only two FT-IR bands at about 580 and 390 cm⁻¹ should be contained. However, it is characterised by three bands, a strong highly asymmetric and broad band at 582 cm⁻¹ and two almost connected bands at 430 and 390 cm⁻¹. The presence of two connected bands in the low wave number region could be explained by a greater sensitivity of this FT-IR region to magnetite nonstoichiometry. There are two possible explanations for the nonstoichiometry of sample M-12, (i) sample M-12 is slightly above-stoichiometric, and (ii) the FT-IR spectrum of sample M-12 shows a short range order nonstoichiometry due to the “memory effect” caused by the reduction process. One can argue that two connected bands in the low wave number region of FT-IR spectra could be due to surface oxidation of the magnetite particles; however the FT-IR spectroscopy in transmission mode is basically insensitive to surface effect.

The reduction of iron oxide by hydrogen gas under static conditions is a more comfortable experiment than working with flow hydrogen gas due to very strict safety rules for laboratory work with hydrogen gas. The main problem encountered with a static condition is condensation of water vapour inside the evacuated glass tube. In order to create a good reduction condition, water vapour should be repeatedly removed (in this work every 30 min) from the glass tube. The formation of water is due to the chemisorption of hydrogen molecules on the iron oxide, which then dissociate from iron oxide generating an intermediate hydroxyl group according to the general equations [25]: $2O^{2-}(s) + H_2(g) \rightarrow 2OH^-(s) + 2e^-$ and $2OH^-(s) \rightarrow O^{2-}(s) + \square_a + H_2O(g)$, where (s) signifies a solid (hematite or substoichiometric magnetite), (g) gas phase, and \square_a an anionic vacancy formed in hematite or substoichiometric magnetite. Similarly, a reduction step $Fe^{3+} \rightarrow Fe^{2+}$ could be regarded as a water desorption step resulting from two hydroxyl group condensation [26].

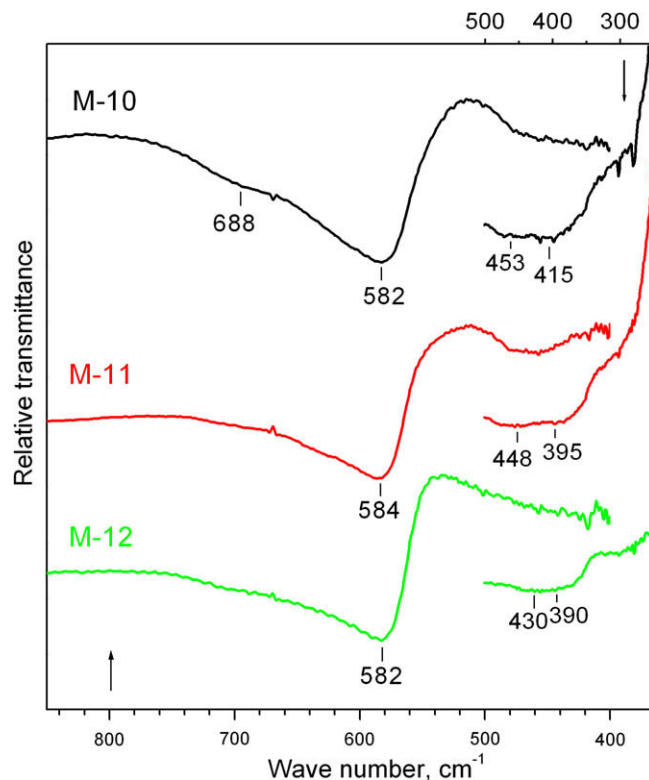
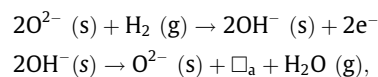


Fig. 10. FT-IR spectra of samples M-10, M-11 and M-12 prepared by the reduction of reference sample M-0 in hydrogen atmosphere under static conditions.

4. Conclusions

- Micrometer-size magnetite particles as a model system were subjected to reduction and reoxidation at a temperature of up to 600 °C.
- XRD and FT-IR spectroscopy indicated the superstructure character of obtained maghemite samples with the ordering of cation vacancies in the maghemite crystal lattice.
- Mössbauer spectroscopy (measured at 20 °C) was highly sensitive to the magnetite stoichiometry, however, it could not detect less than 10 wt% of hematite in a maghemite-hematite mixture.
- During the reduction experiments the experimental conditions for the reduction of reference sample to stoichiometric magnetite (Fe_{3.00}O₄) were found. The reduction was performed by hydrogen gas under static conditions (375 °C, 150 min). Under these static conditions the relatively high amount of water condensed inside the quartz tube was directly observed. The formation of water is due to the chemisorption of hydrogen molecules on the iron oxide, which then dissociate from iron oxide generating an intermediate hydroxyl group according to the general equations:



where (s) signifies a solid (hematite or substoichiometric magnetite), (g) a gas phase, and \square_a an anionic vacancy formed in hematite or substoichiometric magnetite. Thus, in order to ensure a good reduction condition, water vapour was removed from the quartz tube and the tube was refilled with hydrogen gas every 30 min.

Acknowledgments

The authors thank Dr. Anton Drašner for providing equipment for the reduction experiments by hydrogen gas under static conditions and also for contributing to a helpful discussion on the subject.

References

- [1] S. Musić, M. Gotić, S. Popović, *Mater. Lett.* 20 (1994) 143.
- [2] M. Gotić, S. Popović, S. Musić, *Mater. Lett.* 21 (1994) 289.
- [3] M. Gotić, T. Jurkin, S. Musić, *Colloid. Polym. Sci.* 285 (2007) 445.
- [4] M. Gotić, S. Musić, *J. Mol. Struct.* 834–836 (2007) 445.
- [5] M. Gotić, S. Musić, *Eur. J. Inorg. Chem.* (2008) 966.
- [6] A. Ito, M. Shinkai, H. Honda, T. Kobayashi, *J. Biosci. Bioeng.* 100 (2005) 1.
- [7] Q.A. Pankhurst, J. Connolly, S.K. Jones, J. Dobson, *J. Phys. D: Appl. Phys.* 36 (2003) R167.
- [8] C. Sudakar, G.N. Subbanna, T.R.N. Kutty, *J. Phys. Chem. Solids* 64 (2003) 2337.
- [9] M.E. Fleet, *Acta Cryst.* B37 (1981) 917.
- [10] E. Murad, J.H. Johnston, *Iron oxides and oxyhydroxides*, in: G.J. Long (Ed.), *Mössbauer Spectroscopy Applied to Inorganic Chemistry*, Plenum Publishing Corporation, 1990. pp. 507–582.
- [11] J. Tuček, R. Zboril, D. Petridis, *J. Nanosci. Nanotechnol.* 6 (2006) 926.
- [12] J. Tuček, R. Zboril, *J. Phys.* 55 (2005) 1.
- [13] G.M. Da Costa, E. De Grave, A.M. Bryan, L.H. Bowen, *Hyp. Interact.* 94 (1994) 1983.
- [14] G.M. Da Costa, E. De Grave, R.E. Vandenberghe, *Hyp. Interact.* 117 (1999) 207.
- [15] A.N. Shmakov, G.N. Kryukova, S.V. Tsybulya, A.L. Chuvilin, L.P. Solovyeva, *J. Appl. Cryst.* 28 (1995) 141.
- [16] M.P. Morales, C. de Julián, J.M. González, C.J. Serna, *J. Mater. Res.* 9 (1994) 135.
- [17] M. Boudeulle, H. Batis-Landoulsi, CH. Leclercq, P. Vergnon, *J. Solid State Chem.* 48 (1983) 21.
- [18] M.P. Morales, C. Pecharroman, T. Gozalez Carreño, C.J. Serna, *J. Solid State Chem.* 108 (1994) 158.
- [19] M.P. Morales, M. Andres-Vergés, S. Veintemillas-Verdaguer, M.I. Montero, C.J. Serna, *J. Magnet. Magn. Mater.* 203 (1999) 146.
- [20] T. Belin, N. Guigue-Millot, T. Caillot, D. Aymes, J.C. Niepce, *J. Solid State Chem.* 163 (2002) 459.
- [21] A.G. Roca, J.F. Marco, M.P. Morales, C.J. Serna, *J. Phys. Chem. C* 111 (2007) 18577.
- [22] E. De Grave, R.E. Vandenberghe, *Phys. Chem. Miner.* 17 (1990) 344.
- [23] M. Ishii, M. Nakahira, T. Yamanaka, *Solid State Commun.* 11 (1972) 209.
- [24] I. Chamritski, G. Burns, *J. Phys. Chem. B* 109 (2005) 4965.
- [25] E.F. Heald, C.W. Weiss, *Am. Mineral.* 57 (1972) 10.
- [26] W.K. Jozwiak, E. Kaczmarek, T.P. Maniecki, W. Ignaczak, W. Maniukiewicz, *Appl. Catal. A: Gen.* 326 (2007) 17.